Microstructure compatible random field models of heterogeneous materials

George Stefanou[1], Dimitrios Savvas[2] and Panagiotis Gavalas[1]
[1] *Department of Civil Engineering, Aristotle University of Thessaloniki, 54124 Thessaloniki, Greece,* (gstefanou@civil.auth.gr; pgavallas@civil.auth.gr),

[2] *Department of Mechanical Engineering, University of West Attica, 12241 Egaleo,Greece,* (dsavvas@uniwa.gr)

Abstract. A key issue for the determination of the mechanical properties of heterogeneous materials is the existence of a broad range of length scales that govern their behavior. This work presents an effective multiscale computational framework for modeling the spatially varying mechanical properties of heterogeneous materials using random fields derived directly from microstructure images through homogenization combined with the moving window technique. Two applications are provided to illustrate the proposed computational framework. The determination of random fields of bending stiffness properties based on real CT-image data of short fiber composites and the computation of the apparent elasticity tensor of additively manufactured structures with random microstructural defects. The random field models of the first application can be employed for the response variability analysis of composite plates using Monte Carlo simulation. Useful conclusions are derived regarding the effect of scale factor, inter- and intra-layer overlap of printed filament lines on the mesoscale random fields.

Keywords: Heterogeneous Material, Microstructure, Mechanical Properties, Random Field, Response Variability.

1. Introduction

A key issue for the determination of the mechanical properties of heterogeneous materials is the existence of a broad range of length scales that govern their behavior. In the last years, the development of multiscale methods in a stochastic setting for uncertainty quantification and reliability analysis of composite materials and structures is becoming an emerging research frontier. Stochastic multiscale modeling aims to establish a link between the hierarchical models used to simulate the inherent uncertainties of composite materials at various scales (Tal and Fish, 2018). The stochastic multiscale methods for the analysis of heterogeneous materials and structures constitute an extension of the classical deterministic methods to a stochastic framework for the solution of problems with uncertainties in the material properties, geometry and loading. One such method, which has recently received considerable attention, is the stochastic finite element method (SFEM) (Stefanou, 2009). In the framework of SFEM, a random field description of the mechanical properties is usually used. The statistical characteristics of these random fields should be compatible with the material microstructure. To this purpose, there are a few studies in the literature where the random material property fields have been obtained by analyzing directly the microstructure through computational homogenization (Miehe and Koch, 2002; Sena et al., 2013; Tran et al., 2016; Savvas et al., 2016; Sakata et al., 2022; Jetti and Ostoja-Starzewski, 2024).

When it comes to random composites, their homogenized bending properties are also random and quantifying their uncertainty is of great importance. The case of random plate structures, whose stiffness properties are described by random fields, has been investigated in several research works (Choi and Noh, 1996; Chen et al., 2024). In most cases, however, these random fields are not related to composite microstructure. In this work, the effect of microstructure morphology on the bending stiffness properties of short fiber composites is investigated by employing random fields of bending stiffness, which are derived from real microstructure data. ABD matrix homogenization according to classical laminate theory (CLT) is combined with a moving window technique to compute random fields of ABD components from CT image data of a short fiber composite (Gavallas et al., 2025). Appropriate random field models can be selected based on the image-derived data which also account for cross-correlations between different components (Van Bavel et al., 2023) (Section 2).

While homogenization is more commonly associated with the analysis of the mechanical behavior of composite materials, its application in the context of additively manufactured (AM) structures, which usually exhibit significant uncertainties, has been recently reported in the literature (Monaldo and Marfia, 2021; Özen et al., 2021; Somireddy and Czekanski, 2021). However, the aforementioned studies regarding 3D printed parts deal with deterministic homogenized models which do not account for material and geometric uncertainty of the micro/meso-structure. For more realistic modeling, a stochastic approach is needed (Mahadevan et al., 2022), which accounts for the fact that a particular microstructure is just a single sample realization from a specified spatial random process. Monte Carlo (MC) simulation based stochastic homogenization involves the computational analysis of many randomly generated realizations of the heterogeneous medium. The results from these analyses are used to derive its apparent properties and quantify their inherent uncertainties (Ma et al., 2015; Korshunova et al., 2021; Chu et al., 2021; Sakata et al., 2024). In this paper, a cost-effective computational framework is proposed to determine the random fields of the apparent elasticity tensor of AM (FDM printed) structures using the moving window technique and stochastic homogenization based on the extended finite element method (XFEM) coupled with MC simulation (Moës et al., 1999; Savvas et al., 2014). The random spatial variation of the elastic properties of the 3D printed structures is caused by the existence of random microstructural defects. These are due to geometric irregularities in the shape of the pores, which are formed by deviations in the spatial placement of the filament lines. The effect of scale factor, inter- and intra-layer overlap of printed filament lines on the mesoscale random fields is assessed and useful conclusions are derived regarding the degree of variability in different cases (Savvas and Stefanou, 2026) (Section 3).

2. Random fields of bending stiffness of short fiber composites

2.1. Proposed computational framework

In composites that exhibit random inclusion dispersion, spatial variation of the mechanical properties is observed, which can be simulated with random fields. The proposed random field computation procedure can be outlined as follows: An image of the composite is first processed with a moving window of dimensions $L_w \times L_w$, which extracts geometrical information and creates FE models (stochastic volume elements - SVEs) based on local composite morphology, as shown in Fig. 1 (Baxter and Graham, 2000). In the 2D case, the window moves across the x and $y-$ directions at a step of DL_w. For each FE model, homogenization is performed, thus the apparent mechanical properties are computed at each position of the moving window. As a result, a realization of the random fields of mechanical properties can be determined from a single composite image. From this realization, suitable random field models can be selected and response variability analysis can be conducted as in (Stefanou et al., 2017).

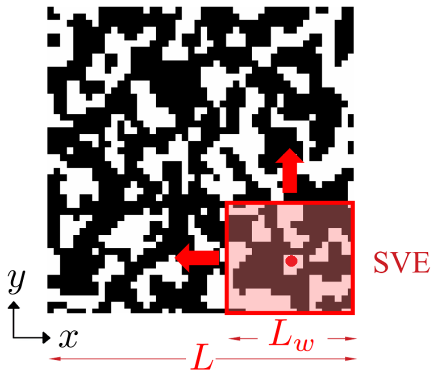

Figure 1. Computer simulated 2D binary image of the microstructure of a composite material, showing fiber (white) and matrix (black) distributions. Illustration of moving window technique and extracted SVE.

Numerical homogenization is performed herein and random fields of the ABD stiffness matrix components are computed (see Appendix). Since different window sizes can lead to different spatial variability, the scale factor $\delta = L_w/d$ is often used to characterize computed random fields at different scales, where d is the inclusion diameter in a fiber reinforced composite. A very large scale factor, which would approach the RVE size, is unlikely to capture the true random response of the material. The scale factor/window size that best describes real material behavior can be determined from experimental data (Guilleminot et al., 2008; Rauter, 2022) and in lack thereof, random fields can be computed for relevant scale factors.

In composites with uniform-like inclusion placement, the resulting random fields can be assumed to be statistically homogeneous. Therefore, the normalized correlation function between ABD stiffness components A and B at a spatial lag (ξ_x^r, ξ_y^s) can be computed through the following equation:

$$\rho(\xi_x^r, \xi_y^s) = \frac{1}{n_x n_y} \sum_{p=1}^{n_x-|r|} \sum_{q=1}^{n_y-|s|} (\frac{A(x_p, y_q) - \overline{A}}{\sigma_A})(\frac{B(x_p + |\xi_x^r|, y_q + |\xi_y^s|) - \overline{B}}{\sigma_B}) \tag{1}$$

where σ_A, σ_B are the standard deviations, $\overline{A}, \overline{B}$ are the spatial average (mean) values of stiffness components A, B and n_x, n_y are the number of windows in the x and $y-$ directions. For the lag indices, it holds that: $-n_x < r < n_x$ and $-n_y < s < n_y$. For $A = B$, the autocorrelation function can be computed from Eq. (1), otherwise cross-correlations are obtained.

2.2. Results and discussion

In this work, real CT image data of a short fiber reinforced composite was employed, in order to compute random fields of the ABD stiffness matrix. The 3D CT data was acquired through the TOMCAT beamline at the Swiss Light Source. It was processed with the RETOMO software of BETA CAE Systems, which resulted in a meshed FE model. A thin slice of this 3D model was processed with the moving window technique, and SVE submodels were selected and homogenized with the proposed method, thus obtaining random fields of the ABD matrix components. ANSA was used for SVE extraction and application of appropriate boundary conditions. Abaqus was employed for solving each boundary value problem and META for result post-processing (BETA CAE Systems, 2024; Dassault Systèmes, 2024).

An epoxy-glass fiber composite is considered, with the following properties: $E_m = 3\ GPa, \nu_m = 0.395$ and $E_{incl} = 73\ GPa, \nu_{incl} = 0.18$. As mentioned previously, a thin slice of the CT model was investigated, with dimensions $L_x \times L_y \times L_z = 1063.4\ \mu m \times 793\ \mu m \times 13\ \mu m$. Random fields for two different scale factors were computed: $\delta = 10$ and $\delta = 20$, which correspond to window sizes $L_w = 52\ \mu m$ and $L_w = 104\ \mu m$, considering an average fiber diameter $d = 5.2\ \mu m$. This required homogenization of 1131 and 266 SVEs, respectively, assuming a window step $DL_w = L_w/2$. The top view of the investigated slice of the material can be seen in Fig. 2(a). Sample SVEs for the two different scale factors can be seen in Fig. 2(b) and Fig. 2(c), with dimensions $L_w \times L_w \times L_z$.

The computed random fields for both extension/shear and bending/torsion components of the ABD matrix of this composite are depicted in Fig. 3. It is clarified that components of the A, B and D matrices in this work are computed in $GPa\ \mu m$, $GPa\ \mu m^2$ and $GPa\ \mu m^3$, respectively, while length quantities are measured in μm.

With regard to the differences between the two scale factors, it is observed that variability decreases at higher scales, as the COV appears to decrease while the opposite is true for the corresponding correlation lengths. One interesting observation is that despite the relatively low stiffness ratio ($E_{incl}/E_m = 24$), the computed random fields of all stiffness components exhibit a high COV, with a maximum of 24.6% at scale factor $\delta = 10$ and 15.2% for $\delta = 20$. This can potentially lead to significant response variability for structures simulated with this material and can be attributed to the large variability of inclusion shapes and orientations in the obtained SVEs.

Additionally, upon close inspection, it becomes apparent that random fields computed from the same type of stresses are also highly correlated with each other. For instance, the random fields of ABD matrix components A_{11} and D_{11} are computed from stress component σ_{xx}, and their plots

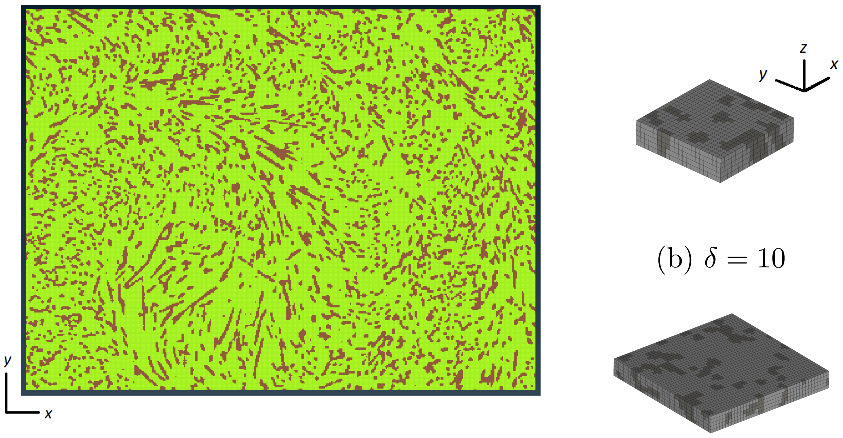

(a) (b) $\delta = 10$ (c) $\delta = 20$

Figure 2. a) Slice of short fiber composite, top view, (b-c) Sample SVEs at different scale factors $\delta = 10$ and $\delta = 20$.

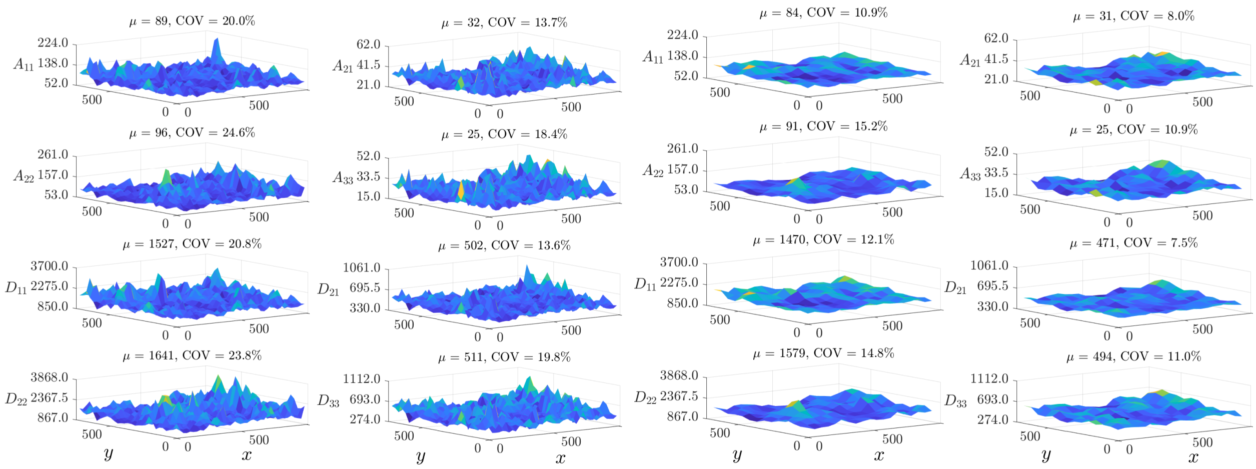

(a) $\delta = 10$. (b) $\delta = 20$.

Figure 3. Random fields of ABD matrix components for the two scale factors.

indicate they are correlated. This is confirmed after calculating the cross-correlation coefficients between all components (Fig. 4), where in this particular case $\rho_{A_{11}}^{D_{11}} = 0.93$. All components appear to be correlated, with the highest correlation being observed for components computed from the same stresses/in the same direction. This suggests that accurate simulation of these random fields for a response variability analysis requires multivariate (cross-correlated) random field models.

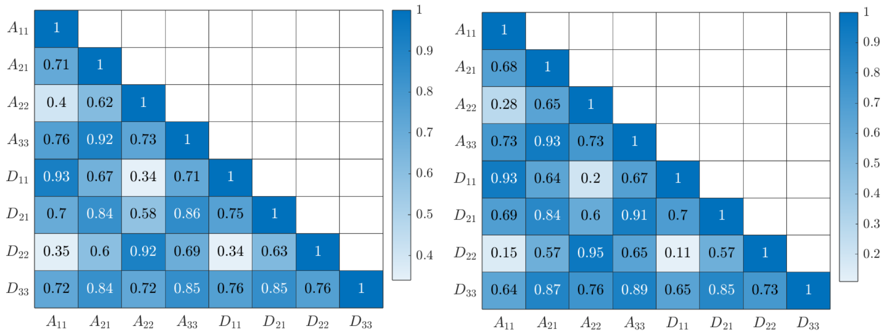

(a) $\delta = 10$ (b) $\delta = 20$

Figure 4. Correlation coefficients ρ for the different components of the ABD matrix.

3. Random fields of apparent elasticity tensor of additively manufactured structures with random microstructural defects

3.1. Proposed computational framework

The additive manufacturing method used in this work is Fused Deposition Modeling (FDM). The main FDM printing parameters that determine the cross-sectional geometry of the printed filament line are shown in Fig. 5(a). The cross section is approximated by an ellipse with major and minor axes of dimensions w and h, respectively. The width w depends on the diameter of the nozzle d_n as $w = 1.1 \times d_n$. Fig. 5(a) illustrates the layer-by-layer construction of the printed object. Ideally, each filament line has no overlap in either the intra- or the inter-layer direction. In this ideal case, the mesostructure of the printed part consists of a unit cell repeated periodically in both directions, defining a deterministic geometry. However, as shown in Fig. 5(b), the mesostructure of a FDM printed object, obtained via scanning electron microscopy (SEM), exhibits uncertainties both in the filament cross-sectional shape and in the spatial placement of each filament line.

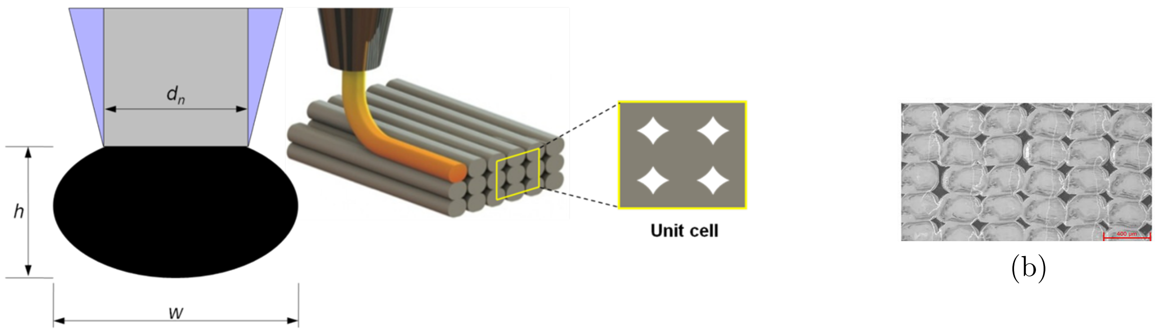

(a) (b)

Figure 5. a) Printing parameters, filament cross-section geometry, layer deposition, and periodic unit cell, b) SEM image of the mesostructure of a FDM printed object.

As explained in Fig. 6, each filament line exhibits a degree of random overlap with its neighboring lines, both in the intra- and inter-layer directions. Consequently, the distances between the centers of the elliptical filament cross sections, d_x and d_y, are stochastic variables given by:

$$\begin{aligned} d_x &= w \cdot (1 - e_x) \\ d_y &= h \cdot (1 - e_y) \end{aligned} \tag{2}$$

where e_x and e_y are stochastic parameters representing the degree of overlap. These parameters are assumed to follow normal distributions with mean value μ and standard deviation σ:

$$\begin{aligned} e_x &\sim N\left(\mu_{e_x}, \sigma_{e_x}^2\right) \\ e_y &\sim N\left(\mu_{e_y}, \sigma_{e_y}^2\right) \end{aligned} \tag{3}$$

The coefficient of variation (COV) can be calculated as the fraction of σ over μ, $COV = \sigma/\mu$.

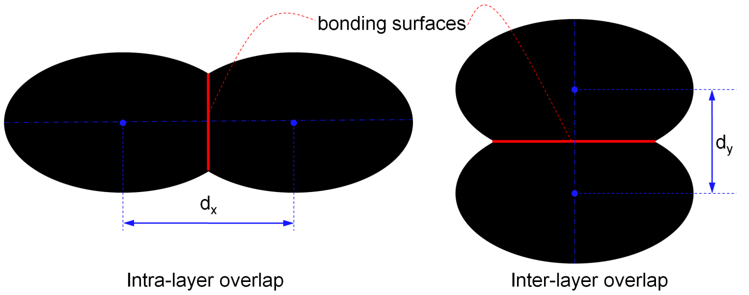

Figure 6. Overlap of printed filament lines in the intra- and inter-layer directions.

In practice, the mesostructure of an AM part exhibits both geometric irregularities in the shape of the cross section of the filament and deviations in spatial placement of the filament lines. These deviations lead to random microstructural defects that affect the mechanical properties of the printed component. To study the influence of these uncertainties, a representative mesostructure case is examined, where the overlap parameters e_x (intra-layer overlap) and e_y (inter-layer overlap) follow normal distributions with mean value μ and standard deviation σ.

The mesostructure image corresponding to this case is generated using the mean value μ and the standard deviation value σ of the overlap parameters, as shown in Fig. 7. The image represents a square region of approximately $L_{im_x} \times L_{im_y} = 35 \times 35\ mm^2$. The printing parameters used to generate this mesostructure image are $d_n = 0.4\ mm$, $w = 0.44\ mm$, and $h = 0.3\ mm$. These stochastic variations in filament positioning form the basis for modeling geometrical uncertainty in subsequent XFEM simulations and homogenization analysis (Savvas and Stefanou, 2026).

3.2. Results and discussion

In this section, random fields for the volume fraction of pores and the apparent elasticity tensor of the 3D printed structure are computed in various mesoscale sizes $\delta = A_w/A_f$ (with A_w the moving window area and A_f the elliptical cross-sectional area of a single filament) based on the simulation of a large number of SVE models extracted using the moving window technique. The computed results

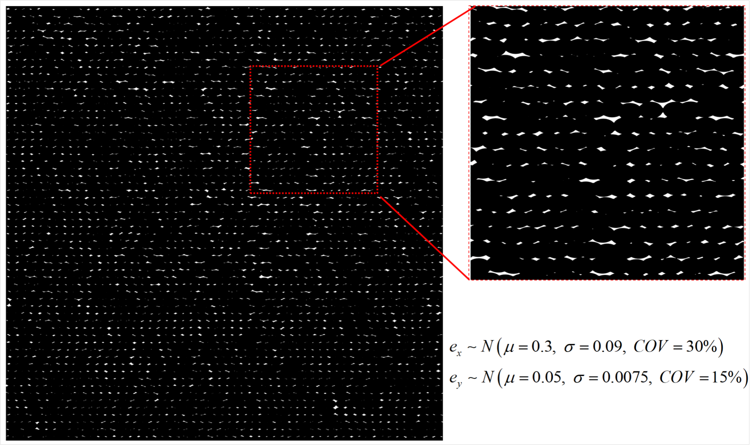

Figure 7. Case of stochastic overlap parameters e_x, e_y.

refer to kinematically uniform boundary conditions (KUBCs) and statically uniform boundary conditions (SUBCs) applied on the 3D printed composite with respect to the statistical properties of the intra- and inter-layer overlap parameters e_x, e_y.

The computed random fields for C_{1111} are shown in Fig. 8 along with their respective empirical probability distributions and autocorrelation functions for the four mesoscale sizes δ examined and for KUBCs. The COV of all mesoscale random fields decreases and their correlation length increases as δ increases. This means that the random fields tend to become less variable and fully correlated as δ increases. The above statistical results are consistent with those obtained in (Sena et al., 2013; Savvas et al., 2016; Sakata et al., 2022; Jetti and Ostoja-Starzewski, 2024) for particle/fiber reinforced and interpenetrating phase composites.

Fig. 9 illustrates the convergence of porosity with respect to δ and the convergence of the upper and lower bounds on the mean values of the axial and shear stiffness properties with respect to δ. A convergence trend is observed as δ increases irrespectively of the type of BCs. It is important to note the large variability of the porosity, particularly at lower scale factors ($COV = 26\%$ for $\delta = 5.67$), which affects significantly the spatial variation of the mechanical properties. In Fig. 9, it can also be observed that the mean value of porosity increases while the COV of porosity decreases with increasing δ. A similar observation can be made on the same figure for the COV values of the apparent mechanical properties C_{ijkl}. The random fields obtained using SUBCs are much more variable than those obtained using KUBCs particularly at small scale factors, which are characterized by larger variability in the porosity.

In addition, the COV of axial stiffness C_{2222} is larger than that of C_{1111}, especially for SUBCs. This behavior can be explained by the relative magnitude of the stochastic overlap parameters. The intra-layer overlap e_x has a relatively large mean value ($\mu_{e_x} = 0.30$), ensuring substantial bonding between filaments within the same layer. Even though its coefficient of variation is higher ($COV = 30\%$), the absolute overlap remains sufficient to maintain effective load transfer along the x-axis, which limits the scatter in the apparent stiffness C_{1111}. In contrast, the inter-layer overlap e_y has a much smaller mean value ($\mu_{e_y} = 0.05$), corresponding to weaker bonding between successive layers. Therefore, small fluctuations around this low mean can produce disproportionately large relative changes in the effective contact area, which amplifies the variability of the apparent stiffness C_{2222}, particularly under SUBCs where weak layer interfaces play a dominant role in stress transfer. A negative correlation between vf and the apparent properties and a strong positive correlation between the various mechanical properties are also observed in Fig. 10, as expected.

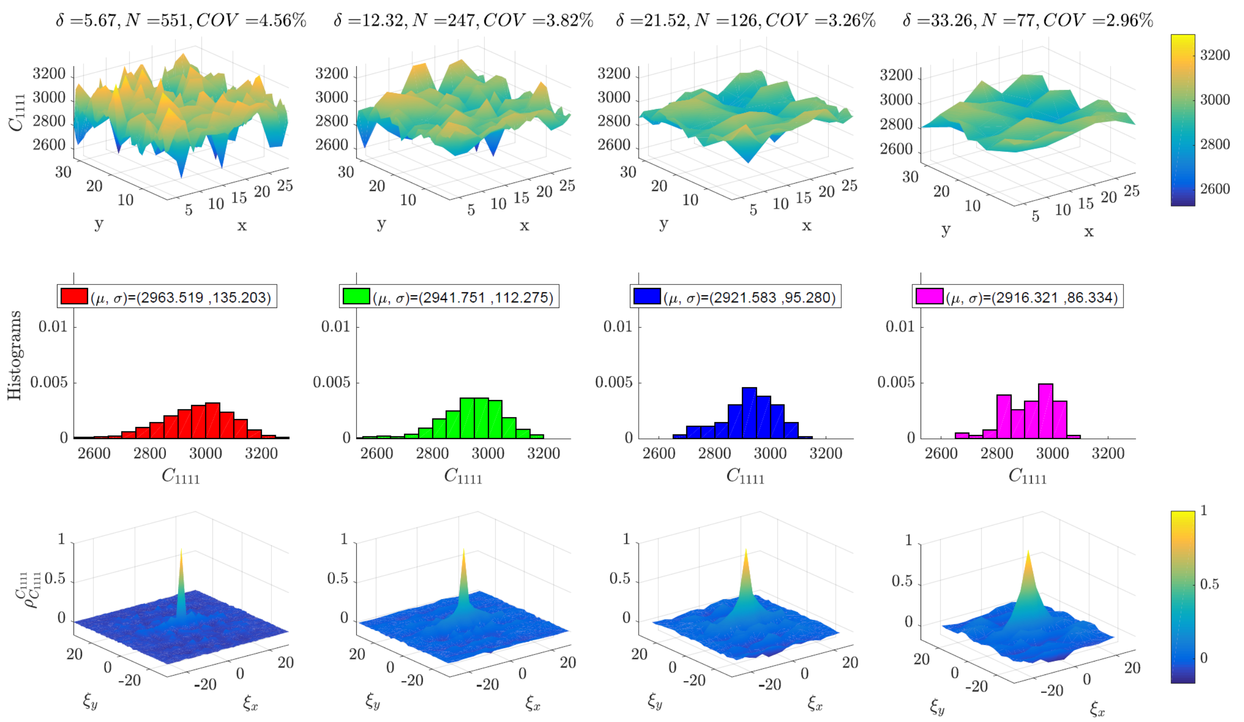

Figure 8. Random fields, empirical probability and autocorrelation functions of axial stiffness C_{1111} for various scale factors δ in case of KUBCs.

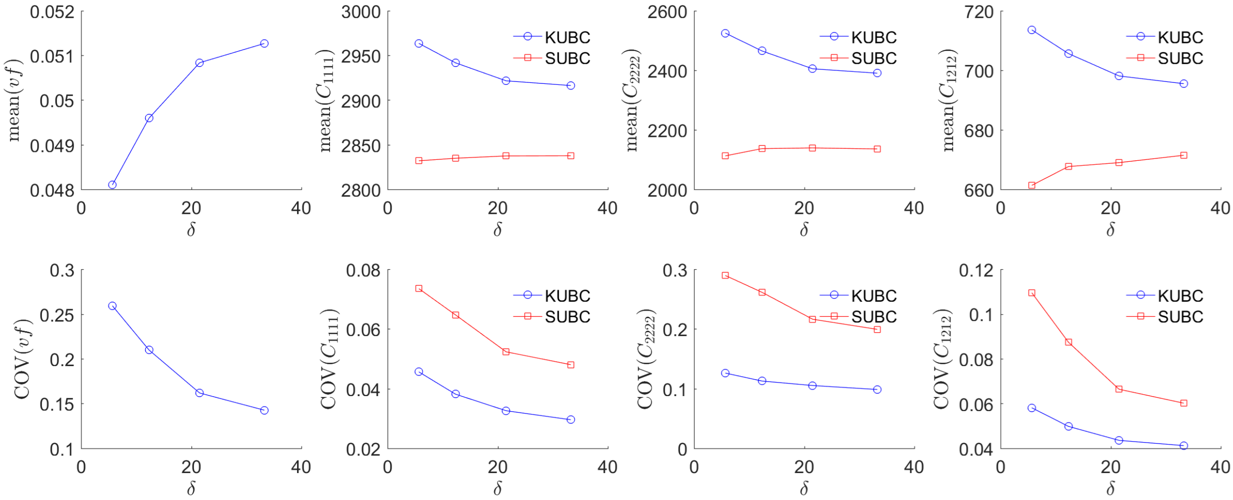

Figure 9. Convergence of mean and COV of porosity, C_{1111}, C_{2222} and C_{1212} with respect to scale factor δ for KUBCs and SUBCs.

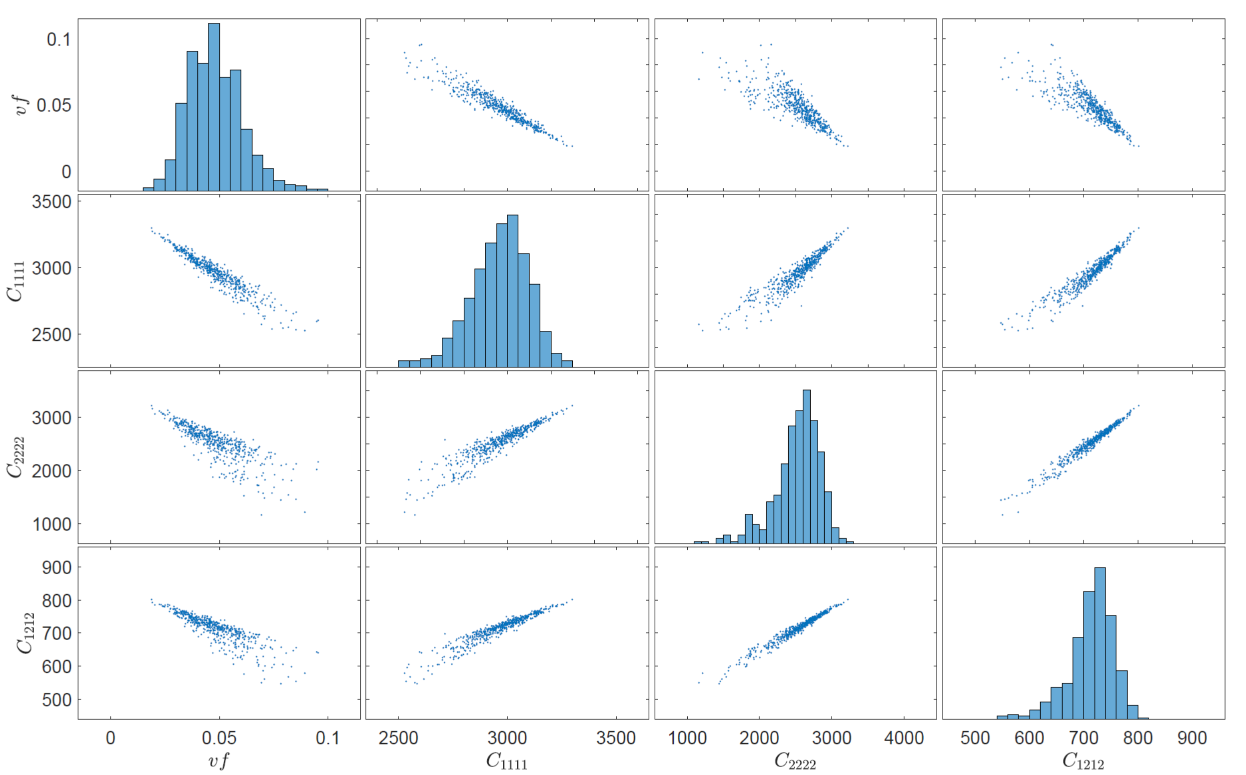

Figure 10. Scatter plots of random porosity and apparent stiffness properties in case of $\delta = 5.67$ and KUBCs.

4. Conclusions

An effective multiscale computational framework was presented for modeling the spatially varying mechanical properties of heterogeneous materials (short fiber composites, additively manufactured structures) using random fields derived directly from microstructure images through homogenization of stochastic volume elements. Based on the numerical results, the following conclusions can be drawn:

- Increasing the mesoscale size δ reduces the variability (COV) of all random fields and increases their correlation length, demonstrating the expected trend towards constant homogenized properties at larger scales.
- Porosity exhibits significant spatial variability at small mesoscale sizes, which strongly influences the stochastic behavior of the elastic moduli of additively manufactured structures.
- Random fields obtained with SUBCs are more variable than those under KUBCs, particularly at small scale factors where the variability of porosity is larger.
- Negative correlations are obtained between porosity and stiffness properties and strong positive correlations between stiffness components, highlighting the effect of microstructural features on the mechanical response.

The computed mesoscale random fields can be employed for the response variability and reliability analysis of structures in the framework of the stochastic finite element method (Gavallas et al., 2025).

Appendix

A. Classical Laminate Theory (CLT)

In CLT, a composite laminate consists of several layers or laminae with different properties or alignment (Agarwal et al., 2006). Each lamina is considered an orthotropic material, therefore its inplane behavior can be described by the following equation:

$$\begin{bmatrix}\sigma_x\\ \sigma_y\\ \tau_{xy}\end{bmatrix} = \begin{bmatrix}C_{11} & C_{12} & 0\\ C_{21} & C_{22} & 0\\ 0 & 0 & C_{33}\end{bmatrix}\begin{bmatrix}\varepsilon_x\\ \varepsilon_y\\ \gamma_{xy}\end{bmatrix} \quad \text{or} \quad \boldsymbol{\sigma} = \mathbf{C}\,\boldsymbol{\varepsilon} \tag{4}$$

where $\mathbf{C}$ is the reduced elasticity matrix under plane stress conditions.

For the computation of the mechanical properties of laminates according to CLT, several assumptions are made. Each lamina is a homogeneous material and there is perfect bonding between each layer. Inplane stiffness is determined by assuming plane stress conditions. With regard to bending behavior, the assumptions of the Kirchoff-Love theory hold, which means that normals to the midplane remain normal and straight, while their lengths do not change. It should be noted that, as the thickness of the laminate increases, the Kirchoff-Love assumptions can lead to inaccurate stiffness estimates.

Under the above assumptions, the relationship between force/moment resultants and mid-surface strains and curvatures according to CLT is given by the following equation:

$$\begin{bmatrix} N_x \\ N_y \\ N_{xy} \\ M_x \\ M_y \\ M_{xy} \end{bmatrix} = \begin{bmatrix} A_{11} & A_{12} & A_{13} & B_{11} & B_{12} & B_{13} \\ A_{21} & A_{22} & A_{23} & B_{21} & B_{22} & B_{23} \\ A_{31} & A_{32} & A_{33} & B_{31} & B_{32} & B_{33} \\ B_{11} & B_{12} & B_{13} & D_{11} & D_{12} & D_{13} \\ B_{21} & B_{22} & B_{23} & D_{21} & D_{22} & D_{23} \\ B_{31} & B_{32} & B_{33} & D_{31} & D_{32} & D_{33} \end{bmatrix} \begin{bmatrix} \varepsilon_x \\ \varepsilon_y \\ \gamma_{xy} \\ \kappa_x \\ \kappa_y \\ \kappa_{xy} \end{bmatrix} \quad \text{or} \quad \begin{bmatrix} \mathbf{N} \\ \mathbf{M} \end{bmatrix} = \begin{bmatrix} \mathbf{A} & \mathbf{B} \\ \mathbf{B} & \mathbf{D} \end{bmatrix} \begin{bmatrix} \boldsymbol{\varepsilon} \\ \boldsymbol{\kappa} \end{bmatrix} \tag{5}$$

where $\mathbf{A}$, $\mathbf{B}$ and $\mathbf{D}$ are called the extensional, coupling and bending stiffness matrices, respectively. Due to the symmetry of the ABD matrix it holds that $A_{ij} = A_{ji},\ B_{ij} = B_{ji}$ and $D_{ij} = D_{ji}$. Note that forces and moments are computed per unit length.

The extensional stiffness matrix $\mathbf{A}$ expresses the relationship between normal/shear forces and midplane strains, while the bending stiffness matrix $\mathbf{D}$ expresses the relationship between bending/torsional moments and plate curvatures. The coupling stiffness matrix $\mathbf{B}$ expresses the interaction between extension and bending, which implies that when components of $\mathbf{B}$ are non-zero, application of normal/shear forces will result in not only midplane strains but also curvatures and plate bending/torsion. It should be noted that in a symmetrical laminate with respect to the midplane, the components of $\mathbf{B}$ will be zero, implying no extension/bending coupling. The $\mathbf{A}$, $\mathbf{B}$ and $\mathbf{D}$ matrices are given by the following equations:

$$A_{ij} = \int_{-\frac{t}{2}}^{\frac{t}{2}} Q_{ij}\,\mathrm{d}z = \sum_{k=1}^{n} Q_{ij}^{(k)}\,(z_k - z_{k-1}) \tag{6}$$

$$B_{ij} = \int_{-\frac{t}{2}}^{\frac{t}{2}} Q_{ij}\,z\,\mathrm{d}z = \frac{1}{2}\sum_{k=1}^{n} Q_{ij}^{(k)}\,(z_k^2 - z_{k-1}^2) \tag{7}$$

$$D_{ij} = \int_{-\frac{t}{2}}^{\frac{t}{2}} Q_{ij}\,z^2\,\mathrm{d}z = \frac{1}{3}\sum_{k=1}^{n} Q_{ij}^{(k)}\,(z_k^3 - z_{k-1}^3) \tag{8}$$

where $Q_{ij}^{(k)}$ is the transformed reduced elasticity matrix of the k-th lamina, t is the total thickness of the laminate, n is the number of laminae and z_k, z_{k-1} are the distances from the mid-surface of the laminate to the inner/outer surfaces of the k-th lamina. In the case that the lamina is aligned with the laminate coordinate system, it holds that $Q_{ij} = C_{ij}$, otherwise transformation of the reduced elasticity matrix C_{ij} is required.

B. Computational homogenization

Computational homogenization is a systematic framework that connects the microscopic responses of heterogeneous materials to their effective macroscopic constitutive behavior, especially under small, linear macroscopic strains and stresses. This method is particularly applied to Representative Volume Elements (RVEs), which characterize the microstructural properties of composite materials (Zohdi and Wriggers, 2008).

The macroscopic strain and stress tensors can be computed as volume averages of the microscopic strain $\varepsilon_{ij}(x, y)$ and stress $\sigma_{ij}(x, y)$ fields which vary throughout the RVE domain B:

$$\bar{\varepsilon}_{ij} = \frac{1}{V} \int_B \varepsilon_{ij}(x, y)\, dB, \tag{9}$$

$$\bar{\sigma}_{ij} = \frac{1}{V} \int_B \sigma_{ij}(x, y)\, dB, \tag{10}$$

where V denotes the RVE volume.

Assuming a linearly elastic anisotropic material, the macroscopic constitutive relation reads:

$$\begin{bmatrix} \bar{\sigma}_{11} \\ \bar{\sigma}_{22} \\ \bar{\sigma}_{12} \end{bmatrix} = \begin{bmatrix} \bar{C}_{1111} & \bar{C}_{1122} & \bar{C}_{1112} \\ & \bar{C}_{2222} & \bar{C}_{2212} \\ sym & & \bar{C}_{1212} \end{bmatrix} \begin{bmatrix} \bar{\varepsilon}_{11} \\ \bar{\varepsilon}_{22} \\ \bar{\varepsilon}_{12} \end{bmatrix} \tag{11}$$

where $\bar{\mathbf{C}}$ is the homogenized stiffness tensor to be determined. It is noted that the microstructure is mechanically inhomogeneous, but a finite volume of the material is assumed to be statistically homogeneous as required by the homogenization technique. Regarding the mesoscale random fields determined by the presented approach, statistical homogeneity and/or isotropy are not assumed, but can emerge based on the underlying microstructure.

References

Agarwal, B. D., L. J. Broutman, and K. Van Breugel: 2006, *Analysis and Performance of Fiber Composites*. John Wiley & Sons.

Baxter, S. C. and L. L. Graham: 2000, 'Characterization of random composites using moving-window technique'. *Journal of Engineering Mechanics* **126**(4), 389–397.

BETA CAE Systems: 2024, 'ANSA, META, and RETOMO [Computer software]'. Accessed: 2025-02-14.

Chen, B., Z. Shao, A. Ademiloye, D. Yang, X. Zhang, and P. Xiang: 2024, 'Stochastic static analysis of functionally graded sandwich nanoplates based on a novel stochastic meshfree computational framework'. *Advances in Engineering Software* **198**, 103780.

Choi, C.-K. and H.-C. Noh: 1996, 'Stochastic finite element analysis of plate structures by weighted integral method'. *Structural Engineering and Mechanics* **4**(6), 703–715.

Chu, S., J. Guilleminot, C. Kelly, B. Abar, and K. Gall: 2021, 'Stochastic modeling and identification of material parameters on structures produced by additive manufacturing'. *Computer Methods in Applied Mechanics and Engineering* **387**, 114166.

Dassault Systèmes: 2024, 'Abaqus [Computer software]'. Accessed: 2025-02-14.

Gavallas, P., G. Stefanou, and E. Tsivolas: 2025, 'The effect of random microstructure morphology on the bending behavior of composite plate structures'. *Composite Structures* p. 119432.

Guilleminot, J., C. Soize, D. Kondo, and C. Binetruy: 2008, 'Theoretical framework and experimental procedure for modelling mesoscopic volume fraction stochastic fluctuations in fiber reinforced composites'. *International Journal of Solids and Structures* **45**(21), 5567–5583.

Jetti, Y. S. and M. Ostoja-Starzewski: 2024, 'Correlation structures of statistically isotropic stiffness and compliance TRFs through upscaling'. *Computer Methods in Applied Mechanics and Engineering* **432**, 117356.

Korshunova, N., I. Papaioannou, S. Kollmannsberger, D. Straub, and E. Rank: 2021, 'Uncertainty quantification of microstructure variability and mechanical behavior of additively manufactured lattice structures'. *Computer Methods in Applied Mechanics and Engineering* **385**, 114049.

Ma, J., S. Sahraee, P. Wriggers, and L. De Lorenzis: 2015, 'Stochastic multiscale homogenization analysis of heterogeneous materials under finite deformations with full uncertainty in the microstructure'. *Computational Mechanics* **55**(5), 819–835.

Mahadevan, S., P. Nath, and Z. Hu: 2022, 'Uncertainty quantification for additive manufacturing process improvement: Recent advances'. *ASCE-ASME Journal of Risk and Uncertainty in Engineering Systems, Part B: Mechanical Engineering* **8**(1), 010801.

Miehe, C. and A. Koch: 2002, 'Computational micro-to-macro transitions of discretized microstructures undergoing small strains'. *Archive of Applied Mechanics* **72**(4-5), 300–317.

Moës, N., J. Dolbow, and T. Belytschko: 1999, 'A finite element method for crack growth without remeshing'. *International Journal for Numerical Methods in Engineering* **46**, 131–150.

Monaldo, E. and S. Marfia: 2021, 'Computational homogenization of 3D printed materials by a reduced order model'. *International Journal of Mechanical Sciences* **197**, 106332.

Özen, A., B. E. Abali, C. Völlmecke, J. Gerstel, and D. Auhl: 2021, 'Exploring the role of manufacturing parameters on microstructure and mechanical properties in fused deposition modeling (FDM) using PETG'. *Applied Composite Materials* **28**(6), 1799–1828.

Rauter, N.: 2022, 'Numerical Simulation of the Elastic-Ideal Plastic Material Behavior of Short Fiber-Reinforced Composites Including Its Spatial Distribution with an Experimental Validation'. *Applied Sciences* **12**(20), 10483.

Sakata, S.-i., G. Stefanou, and S. Araki: 2022, 'Random field modeling of local strength of a randomly arranged unidirectional fiber-reinforced composite material under transverse tensile loading'. *Materials Today Communications* **33**, 104783.

Sakata, S.-i., G. Stefanou, T. Kikkawa, and Y. Aikawa: 2024, 'Probabilistic analysis of homogenized elastic property for resin products fabricated by additive manufacturing based on three-dimensional random field modeling of microstructure'. *Mechanics of Materials* **196**, 105071.

Savvas, D. and G. Stefanou: 2026, 'Determination of the mechanical properties of additively manufactured structures with random microstructural defects'. *Computer Methods in Applied Mechanics and Engineering* **449**, 118574.

Savvas, D., G. Stefanou, and M. Papadrakakis: 2016, 'Determination of RVE size for random composites with local volume fraction variation'. *Computer Methods in Applied Mechanics and Engineering* **305**, 340–358.

Savvas, D., G. Stefanou, M. Papadrakakis, and G. Deodatis: 2014, 'Homogenization of random heterogeneous media with inclusions of arbitrary shape modeled by XFEM'. *Computational mechanics* **54**(5), 1221–1235.

Sena, M. P., M. Ostoja-Starzewski, and L. Costa: 2013, 'Stiffness tensor random fields through upscaling of planar random materials'. *Probabilistic Engineering Mechanics* **34**, 131–156.

Somireddy, M. and A. Czekanski: 2021, 'Computational modeling of constitutive behaviour of 3D printed composite structures'. *Journal of Materials Research and Technology* **11**, 1710–1718.

Stefanou, G.: 2009, 'The stochastic finite element method: Past, present and future'. *Computer methods in applied mechanics and engineering* **198**(9-12), 1031–1051.

Stefanou, G., D. Savvas, and M. Papadrakakis: 2017, 'Stochastic finite element analysis of composite structures based on mesoscale random fields of material properties'. *Computer Methods in Applied Mechanics and Engineering* **326**, 319–337.

Tal, D. and J. Fish: 2018, 'Stochastic multiscale modeling and simulation framework for concrete'. *Cement and Concrete Composites* **90**, 61–81.

Tran, V., J. Guilleminot, S. Brisard, and K. Sab: 2016, 'Stochastic modeling of mesoscopic elasticity random field'. *Mechanics of Materials* **93**, 1–12.

Van Bavel, B., Y. Zhao, M. Faes, D. Vandepitte, and D. Moens: 2023, 'Efficient quantification of composite spatial variability: A multiscale framework that captures intercorrelation'. *Composite Structures* **323**, 117462.

Zohdi, T. I. and P. Wriggers: 2008, *An Introduction to Computational Micromechanics, 2nd Edition, Lecture Notes in Applied and Computational Mechanics*, Vol. 20. Springer, Heidelberg.